energies

MDPI

Article

Numerical Modeling of CO_2, Water, Sodium Chloride, and Magnesium Carbonates Equilibrium to High Temperature and Pressure

Jun Li * and Xiaochun Li

State Key Laboratory of Geomechanics and Geotechnical Engineering, Institute of Rock and Soil Mechanics, Chinese Academy of Sciences, Wuhan 430071, China; xcli@whrsm.ac.cn

* Correspondence: lijun2009s@gmail.com

Received: 26 September 2019; Accepted: 27 November 2019; Published: 28 November 2019

Abstract: In this work, a thermodynamic model of CO_2-H_2O-NaCl-$MgCO_3$ systems is developed. The new model is applicable for 0–200 °C, 1–1000 bar and halite concentration up to saturation. The Pitzer model is used to calculate aqueous species activity coefficients and the Peng–Robinson model is used to calculate fugacity coefficients of gaseous phase species. Non-linear equations of chemical potentials, mass conservation, and charge conservation are solved by successive substitution method to achieve phase existence, species molality, pH of water, etc., at equilibrium conditions. From the calculated results of CO_2-H_2O-NaCl-$MgCO_3$ systems with the new model, it can be concluded that (1) temperature effects are different for different $MgCO_3$ minerals; landfordite solubility increases with temperature; with temperature increasing, nesquehonite solubility decreases first and then increases at given pressure; (2) CO_2 dissolution in water can significantly enhance the dissolution of $MgCO_3$ minerals, while $MgCO_3$ influences on CO_2 solubility can be ignored; (3) $MgCO_3$ dissolution in water will buffer the pH reduction due to CO_2 dissolution.

Keywords: thermodynamic modeling; CO_2 storage; $MgCO_3$ minerals; phase behaviors; mineral solubility; CO_2 solubility

1. Introduction

CO_2 geological storage has been proved as an important option to reduce carbon emission and a clean way of using fossil energy resources [1]. When CO_2 is injected into underground reservoirs, the reactions of CO_2, water and various minerals are activated [2]. Magnesium carbonates are commonly found minerals in geological reservoirs. A reliable thermodynamic model of CO_2, brine, and magnesium carbonate minerals is essential to understand phase behavior, water property changes, and mineral participation and dissolution [3]. Further, it will help us to understand the reservoir property (porosity and permeability) change after CO_2 injected. Numerical dynamic simulation of the fluid migration process is usually an important tool to analyze the whole procedure and helps the decision making of a real CO_2 storage project [4]. The thermodynamic model is one of the basic components in a simulation framework.

Both magnesium and carbon are commonly found underground in terms of various kinds of minerals. Researchers started experimental work on the H_2O-$MgCO_3$ system in 1867 [5]. Wagner [5] measured magnesite solubility at 5 °C and with CO_2 partial pressure from 1 to 6 atm. The followers conducted magnesite solubility measurements with temperature up to 91 °C and CO_2 partial pressure up to about 10 atm [5–12]. Cameron and Seidel [12] measured magnesite solubility in NaCl solutions with NaCl molality up to 6.5 molal. Nesquehonite solubility in water was first measured by Engel et al. [13]. The most recent measurements were carried out by Konigsberger et al. [14]. The temperature range of the experiments is from 0–90 °C and CO_2 partial pressure ranges from about 0 to 56 atm [7,10,14–18]. Lansfordite solubility experiment work is less than magnesite and nesquehonite. The available literatures are Takahashi et al. [19], Ponizonvskii et al. [20], and Yanat'eva and Rassonskaya [21]. The temperature of the experiments is less than 15 °C and pressure is less than 10 atm. Numerical modeling of CO_2-brine-salts-minerals was started in the 1980s. The pioneer work is from Harvie and Weare [22] and Harvie et al. [23]. They developed series thermodynamic models of sea water components based on the Pitzer model [24–27]. The models are able to accurately predict mineral precipitation and dissolution. The temperature and pressure are at standard condition (25 °C and 1 atm). Moller [28], Moller and Greenberg [29], and Christov and Moller [30] modeled temperature effects on the system. Duan and co-workers focused on the pressure effects and developed models on CO_2-H2O-NaCl-$CaCO_3$-CaSO4 systems from standard condition to high temperatures and pressures [31–34]. Thermodynamic models have been implemented in research or commercial software on reactive transport. The most famous reactive transport software packages are PhreeqC [35], TOUGHREACT [36], MIN3P [37], and EQ3/6 [38]. They have shown success in real project applications [39–41]. Some commercial reservoir simulators have coupled the reactive transport module (such as CMG-GEM [42] and MoReS-PhreeqC [43]) and were successfully applied in enhanced oil recovery research or real projects [44,45].

In this work, a new thermodynamic model of CO_2-H_2O-NaCl-$MgCO_3$ systems is developed. The model is based on the existing experimental data and the consistency checking. The $MgCO_3$ minerals of magnesite, nesquehonite, and lansfordite are considered in the system. In Section 2, the methodology of the thermodynamic modeling is introduced. In Section 3, model validations are made by comparing the model results and available experimental data of the systems. In Section 4, the model is used to predict $MgCO_3$ mineral solubility, aqueous solution properties (such as pH and various carbon ion concentrations) at various conditions. The influences of CO_2 and $MgCO_3$ on the speciation in the solutions are evaluated by the model.

2. Phenomenological Description and Geochemical Modeling

When a system of CO_2-H_2O-NaCl-$MgCO_3$ approaches equilibrium at given temperature and pressure, phases of solids, vapor, and brine (aqueous phase) can appear. Minerals of magnesite ($MgCO_3$), nesquehonite ($MgCO_3 \cdot 3H_2O$), and lansfordite ($MgCO_3 \cdot 5H_2O$) are considered in this modeling work. The salt of sodium chloride (NaCl) can be precipitated when NaCl becomes saturated in the aqueous phase. In the vapor phase, the possible components are CO_2 and H_2O. In the aqueous phase, various cations, anions, and neutral particles can be dissolved. The following reversible reactions are considered for the modeling:

$$H_2O^{(aq)} \leftrightarrow H_2O^{(g)}, \tag{1}$$

$$CO_2{}^{(aq)} \leftrightarrow CO_2{}^{(g)}, \tag{2}$$

$$CO_2{}^{(aq)} + H_2O^{(aq)} \leftrightarrow CO_3{}^{2-} + 2H^+, \tag{3}$$

$$H_2O \leftrightarrow H^+ + OH^-, \tag{4}$$

$$HCO_3{}^- \leftrightarrow CO_3{}^{2-} + H^+, \tag{5}$$

$$NaCl^{(s)} \leftrightarrow Na^+ + Cl^-, \tag{6}$$

$$MgCO_3{}^{(s,Magnesite)} \leftrightarrow CO_3{}^{2-} + Mg^{2+}, \tag{7}$$

$$MgCO_3 \cdot 3H_2O^{(s,Nesquehonite)} \leftrightarrow Mg^{2+} + CO_3{}^{2-} + 3H_2O, \tag{8}$$

$$MgCO_3 \cdot 5H_2O^{(s,Lansfordite)} \leftrightarrow Mg^{2+} + CO_3{}^{2-} + 5H_2O, \tag{9}$$

$$MgCO_3{}^{(aq)} \leftrightarrow Mg^{2+} + CO_3{}^{2-}, \tag{10}$$

$$Mg^{2+} + H_2O = MgOH^+ + H^+, \tag{11}$$

where (*aq*) denotes aqueous species; *(s)* denotes solid phase; *(g)* denotes gaseous phase species. When the whole system reaches equilibrium state, each of the above reactions will have:

$$\sum_r \nu_{ri}\mu_{ri} = 0, \tag{12}$$

where μ_{ri} is the chemical potential for reaction r and species i; ν_{ri} is the stoichiometric coefficient of species i in reaction r.

For aqueous species,

$$\mu_i = \mu_i^0 + RT\ln(m_i\gamma_i). \tag{13}$$

For gaseous species,

$$\mu_i = \mu_i^0 + RT\ln(x_iP\varphi_i), \tag{14}$$

where μ_i^0 is standard chemical potential at the reference state; m_i is the molality of aqueous species i; γ_i is the activity coefficient of aqueous species i; x_i is mole fraction of gaseous species i; φ_i is fugacity coefficient of gaseous species i; P is total gas pressure; R is gas constant; T is temperature. More details about the parameter definition can be found from Duan and Li [32] and Li and Duan [34]. With Equations (12)–(14), equilibrium constant is usually defined for each chemical reaction as follows:

$$\ln K_r = -\frac{\sum_i \nu_{ri}\mu_{ri}^0}{RT}. \tag{15}$$

Combined with definition of chemical potential, we have:

$$K_r = \Pi {a_{ri}}^{\nu_{ri}} \tag{16}$$

Here, a_{ri} is activity for aqueous species ($m_{ri}\gamma_{ri}$) and fugacity for gaseous phase ($x_{ri}P\varphi_{ri}$). The thermodynamic modeling of the system is to determine the equilibrium constants, activity, and fugacity of each reaction. We follow the model from our previous work from Li et al. [46] for reactions (1) and (2), and from Li and Duan [34] for reactions (3) to (6).

2.1. Equilibrium Constant

The equilibrium constant can be further expressed as [33,34]:

$$K_i = K(T, P_{ref})\exp\left(\frac{\overline{V_{m,i}}(P - P_{ref})}{RT}\right), \tag{17}$$

where $K(T, P_{ref})$ is equilibrium constant at reference pressure P_{ref}; the reference pressure is usually 1 bar at temperature under 373.15 K, and vapor pressure of water above 373.15 K; $\overline{V_{m,i}}$ is molar volume of aqueous species i. For $K(T, P_{ref})$, we follow the empirical equation from Appelo [47]:

$$\log(K_H(T, P_{ref})) = A_0 + A_1T + \frac{A_2}{T} + A_3\log(T) + \frac{A_4}{T^2} + A_5T^2. \tag{18}$$

For reactions (7) to (9), we regressed the parameters in Equation (17) and $\overline{V_{m,i}}$ from the related mineral solubility in water or brine. $\overline{V_{m,i}}$ is calculated as follows:

$$\overline{V_{m,i}} = 41.84\left(0.1a_{1,i} + \frac{100a_{2,i}}{2600 + P} + \frac{a_{3,i}}{(T - 288)} + \frac{10^4a_{4,i}}{(2600 + P)(T - 288)} - \omega_i \times QBrn\right), \tag{19}$$

where $a_{1,i}$–$a_{4,i}$ and ω_i are the parameters found in Appelo [47], and $QBrn$ is the Born function, which can be found in Helgson et al. [48]. For magnesium carbonate dissolution reactions (7–9), we assume

$\overline{V_{m,i}}$ is set as a constant value. For reactions (10) and (11), $\overline{V_{m,i}}$ is calculated following Helgson et al. [48]. Table 1 shows the parameters used in this model.

Table 1. Parameters of equilibrium constants for magnesium carbonate dissolution reactions.

Reaction	A_0	A_1	A_2	A_3	A_4	A_5	$\overline{V_m}$
(7)	7.267	−0.033918	−1476.604	0	0	0	28.3
(8)	−6.008	−0.00688	873.4	0	0	0	74.789
(9)	−4.85	0	0	0	0	0	100.81
(10)	−0.5837	−9.2067	−2.3984	−0.03	0	0	Helgson et al. [48]
(11) [a]	−11.809	0	0	0	0	0	0

[a] From Appelo [47].

2.2. Activity Model and Fugacity Model

From Equation (13), the activity coefficient describes the deviation of an aqueous species in a real solution from that in ideal solution. Pitzer [24] proposed an accurate model framework that can accurately estimate the activity coefficients of aqueous species and osmotic coefficients of H2O in solutions to high salinity. Science 1980s, the Pitzer model [24] framework began to be used to model water–salt–mineral equilibria with various kinds of aqueous species (Harvie and Weare [22]; Harvie et al. [23]; Greenburg et al. [29]; Moller [28]; Christov and Moller [30]; Li and Duan [33]) and shows its success in applications. Li and Duan [34] and many other literatures [29–33] provided the expressions of the model in details. In this work, we use the Pitzer model to calculate the activity coefficients. The Pitzer parameters includes cation and anion binary interaction parameters $\beta^{(0)}_{c,a}$, $\beta^{(1)}_{c,a}$, $C^{\varphi}_{c,a}$, cation and cation binary interaction parameters $\theta_{c,c}$, anion and anion interaction parameters $\theta_{a,a}$, triple particle interaction parameters $\Psi_{c,c,a}$, $\Psi_{c,a,a}$, and neutral-ion interaction parameters λ_{n-a}, λ_{n-c}. The selection of the Pitzer parameters can be found from Table 2.

Table 2. The Pitzer parameters of the system.

$\beta^{(0)}_{CO_3^{2-},Na^+}$, $\beta^{(0)}_{HCO_3^-,Na^+}$, $\beta^{(0)}_{Cl^-,Na^+}$, $\beta^{(1)}_{Cl^-,Na^+}$, $\beta^{(1)}_{CO_3^{2-},Na^+}$, $\beta^{(1)}_{HCO_3^-,Na^+}$, $\beta^{(0)}_{OH^-,Na^+}$, $\beta^{(1)}_{OH^-,Na^+}$, $C^{\varphi}_{CO_3^{2-},Na^+}$, $C^{\varphi}_{HCO_3^-,Na^+}$, $C^{\varphi}_{Cl^-,Na^+}$, $C^{\varphi}_{OH^-,Na^+}$, Ψ_{Cl^-,HCO_3^-,Na^+}, Ψ_{Cl^-,OH^-,Na^+}, Ψ_{Cl^-,H^+,Na^+}	Li and Duan [33], Duan and Li [32]
$\beta^{(0)}_{CO_3^{2-},Mg^{2+}}$, $\beta^{(0)}_{HCO_3^-,Mg^{2+}}$, $\beta^{(0)}_{Cl^-,Mg^{2+}}$, $\beta^{(1)}_{Cl^-,Mg^{2+}}$, $\beta^{(1)}_{CO_3^{2-},Mg^{2+}}$, $\beta^{(1)}_{HCO_3^-,Mg^{2+}}$, $\beta^{(0)}_{OH^-,Mg^{2+}}$, $\beta^{(1)}_{OH^-,Mg^{2+}}$, $C^{\varphi}_{CO_3^{2-},Mg^{2+}}$, $C^{\varphi}_{HCO_3^-,Mg^{2+}}$, $C^{\varphi}_{Cl^-,Mg^{2+}}$, $C^{\varphi}_{OH^-,Mg^{2+}}$, $\Psi_{Cl^-,HCO_3^-,Mg^{2+}}$, $\Psi_{Cl^-,OH^-,Mg^{2+}}$, $\Psi_{Cl^-,H^+,Mg^{2+}}$	Greenburg et al. [29]; Moller 1988 [28] Christov and Moller [30];
$\Psi_{Cl^-,OH^-,Mg(OH)^+}$, $\Psi_{Cl^-,H^+,Mg(OH)^+}$, $\beta^{(0)}_{Cl^-,Mg(OH)^+}$, $\beta^{(1)}_{Cl^-,Mg(OH)^+}$, $\beta^{(0)}_{HCO_3^-,Mg(OH)^+}$, $\beta^{(1)}_{CO_3^{2-},Mg(OH)^+}$	Set to 0.0
λ_{CO2,Na^+}, $\lambda_{CO2,Mg^{2+}}$, $\lambda_{CO2,CO3^{2-}}$, λ_{CO2,HCO_3^-}	Duan and Sun [31]; Duan et al. [49]

To calculate the fugacity coefficient of gaseous component (CO_2 and H_2O), the Peng–Robinson (PR) model [50] is used. The details of the PR model and the methodology of the application are discussed in our previous work [2,46]. The equation for PR model is as follows:

$$P = \frac{RT}{V_m - b} - \frac{a(T)}{V_m(V_m + b) + b(V_m - b)} \tag{20}$$

where $a(T) = a(T_c)\alpha(T_r, \omega)$; $a(T_c)$ is the Van der Waals' attraction factor at a critical temperature defined as $a(T_c) = 0.45724\frac{R^2T_c^2}{P_c}$, where P_c is critical pressure; $b = 0.07780\frac{RT_c}{P_c}$; T_r is reduced temperature

$T_r = \frac{T}{T_c}$; T_c is critical temperature; ω is acentric factor; $\alpha(T_r, \omega)$ is a dimensionless function of relative temperature and acentric factor.

When gaseous phase has more than one component, the mixing rule is considered for parameters "a" and "b":

$$a = \sum_i \sum_j y_i y_j a_{ij}, \tag{21}$$

$$b = \sum_i b_i y_i, \tag{22}$$

where $a_{ij} = \sqrt{a_i a_j}(1 - \delta_{ij})$ and δ_{ij} is binary interaction coefficient of species i and j; y_i is mole fraction of species i in gaseous phase. The PR parameters are adopted from Li et al. [46].

2.3. Calculation Routine

The equilibrium of the whole system is described by equations of chemical potentials, charge and mass conservation. The equations are non-linear. In this work, we use successive substitution method (Li and Duan [34]; Michealson and Mollerup [51]). The calculation routine is as follows.

(1) Initialize the system with molality of each component and species at given pressure and temperature.
(2) Calculate the equilibrium constant of each reaction.
(3) Calculate activity coefficient of each aqueous species and fugacity coefficient of each gaseous species with current molality of each species of the system.
(4) Solve mass and charge conservation equations and linearized reaction equilibrium equations. Update the molality and activity/fugacity coefficient of each species.
(5) Calculate the absolute relative difference of molality of each species and activity coefficient. If both are smaller than tolerance, stop the calculation and output the final results. Otherwise, go to step (3).

3. Results

3.1. Comparisons of $MgCO_3$ Mineral Solubility: Model Calculations and Experiments

The experimental work of $MgCO_3$ mineral solubility started very early by previous researchers [5–8]. However, the reliable experimental data of this system is not sufficient for modeling. To test the model behavior, we compared the model results with the existing experimental data of $MgCO_3$ mineral solubility. Visscher et al. [52] carefully compared the experimental data and checked the reliability of the data. We defined average absolute deviation (*AAD*) to measure the difference between model results and experimental work:

$$AAD\% = \frac{1}{N} \sum \left| \frac{s_{cal} - s_{\exp}}{s_{\exp}} \right| \times 100\%, \tag{23}$$

where N denotes the number of data points; S_{cal} denotes calculated solubility; S_{exp} denotes experimental solubility.

Table 3 shows the experimental data of magnesite ($MgCO_3$) in water and the average absolute deviation of the calculated results from this model. The experimental data of magnesite are usually at temperature from normal temperature to 91 °C and CO_2 partial pressure to about 1 atm. More recent work is from Benezeth et al. [3] who conducted experiments of magnesite solubility with temperature from 120 to 200 °C and CO_2 partial pressure from 12–30 bar. From the comparison, the *AAD*% is usually less than 10% with some of them up to 13.17%. Figure 1 shows the magnesite solubility trend with temperature at various CO_2 partial pressure calculated by this model. The trend shows that the model results are reliable compared with the experimental data.

Table 3. Average absolute deviation of magnesite solubility in water between model calculation by this model and the experimental results.

Reference	Data Points	T (°C)	P_{CO2} (atm)	*AAD%*
Wells [7]	1	20	0.00029	3.8
Bar [8]	2	18	0.00031	13.3
Halla [9]	2	25–38.8	0.932–0.955	8.75
Berg and Borisova [10]	1	25	0.987	11.6
Christ and Hostetler [11]	3	90.3–91	0.0274–0.312	9.61
Benezeth et al. [3]	11	120–200	12–30	13.17

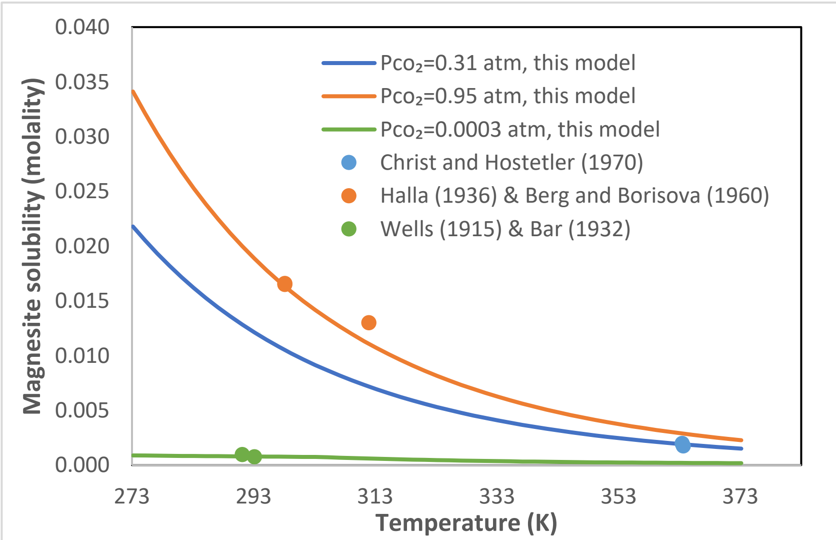

Figure 1. Comparison of magnesite solubility in water at various temperatures and pressures. Lines are calculated results by this model, and dots are from experiments.

The experimental data of nesquehonite solubility in water is more than that of magnesite, but is with limited TP range. The temperature is from 0 to 60 °C and CO_2 partial pressure is from 0.00029 to 21 atm. Table 4 shows the comparison between experimental data and the calculated results by this model. The average absolute deviations are all under 10%. Figure 2a posts all of the experimental data (which are judged as reliable by Visscher et al. [52]) and the calculated results with dots, most of which are quite close to the equal line (y = x). Figure 2b shows the nesquehonite solubility varying with CO_2 partial pressure at various temperature. The comparison shows a reliable nesquehonite solubility trend with CO_2 partial pressure with this model calculations.

Table 4. Average absolute deviation of nesquehonite solubility in water between model calculation by this model and the experimental results.

Reference	Data Points	T (°C)	P_{CO2} (atm)	*AAD%*
Engel [13]	14	3.5–50	0.878–5.986	2.09
Wells [7]	2	20	0.00029	9.41
Mitchell [16]	6	25	6–21	5.22
Haehnel [17]	12	5–60	1	1.13
Yanat and Rassonskaya [21]	10	0–53.5	1	2.91

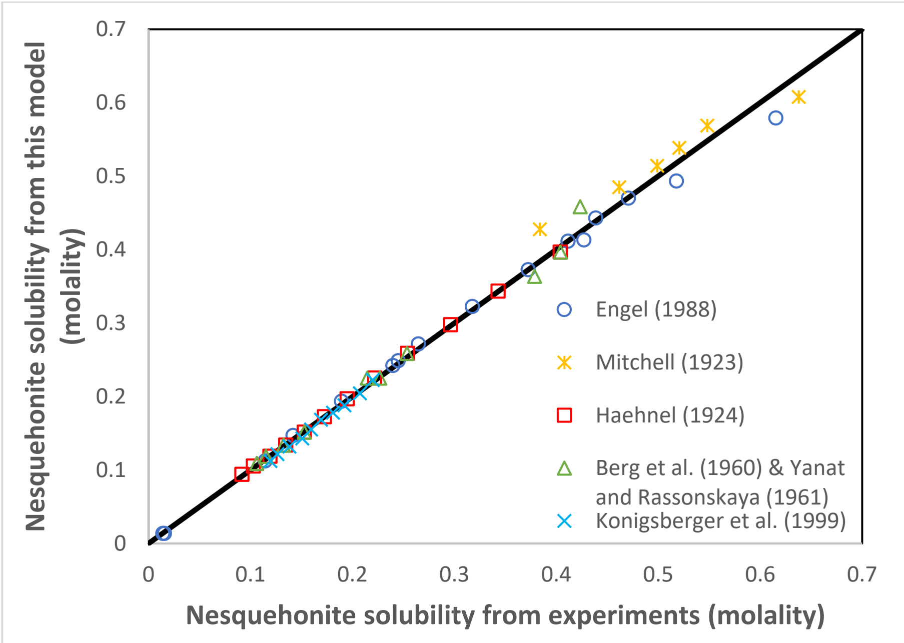

(**a**)

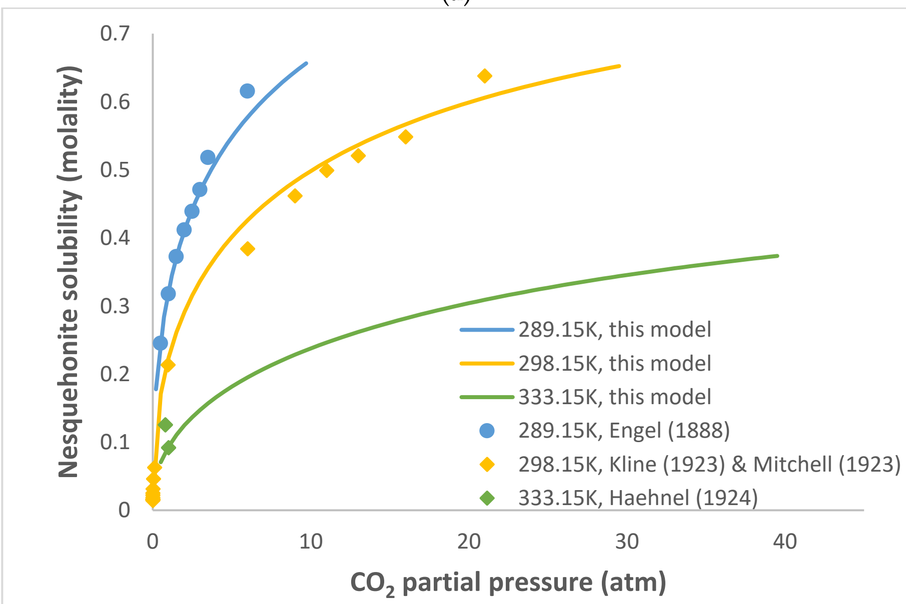

(**b**)

Figure 2. Comparison of nesquehonite solubility in water at various temperatures and pressures between calculated results by this model and experiments. Dots are experimental data from references [10,13–17], and lines are calculated results by this model. (**a**) comparison of experimental nesquehonite solubility in water and the calculated results by this model. (**b**) Nesquehonite solubility varying with CO_2 partial pressure at various temperatures.

Compared with magnesite and nesquehonite, the experimental data of lansfordite solubility in water is even less. The experimental work covers the temperature range from −1.8 to 20 °C and CO_2 partial pressure from 1–10 atm. Table 5 shows the average absolute deviation of the calculated results with this model from the current available experimental data. From the comparison, the calculated results are close to the experimental data. Figure 3 shows the lansfordite solubility varying with temperature at various CO_2 partial pressures. The available experimental data points are also post on the figure. The model results show its reliability to predict the solubility trend.

Table 5. Average absolute deviation of lansfordite solubility in water between model calculation by this model and the experimental results.

Reference	Data Points	T (°C)	P_{CO2} (atm)	*AAD%*
Takahashi et al. [19]	6	−1.8–20	0.987	1.84
Ponizonvskii et al. [20]	4	0	1.93–9.68	3.92
Yanat'eva and Rassonskaya [21]	3	0–15	1	7.11

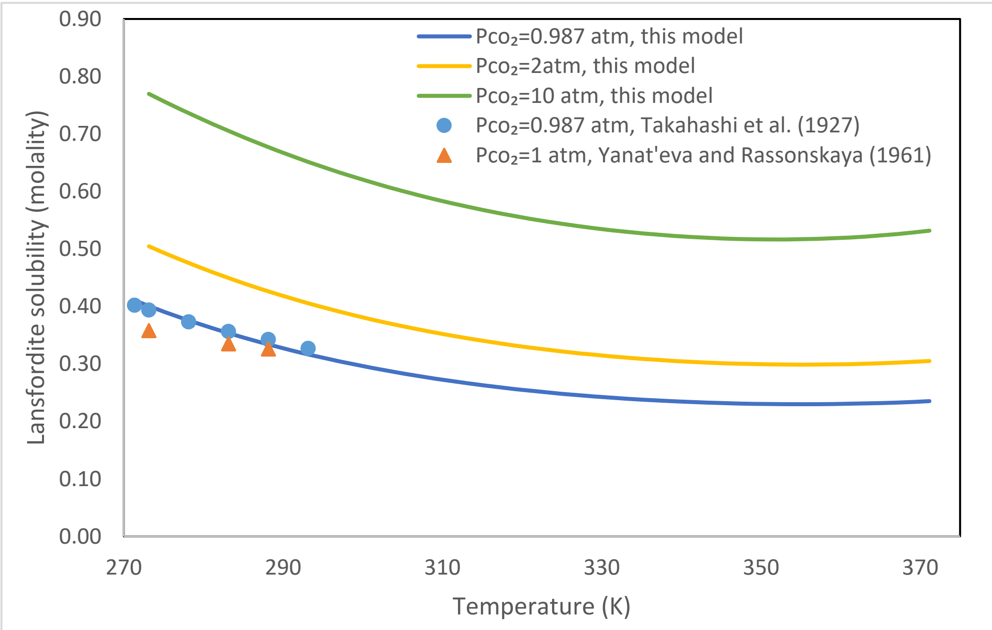

Figure 3. Comparison of lansfordite solubility in water at various temperatures and pressures. Line is the calculated results by this model and dots are from experiments.

3.2. CO_2 Solubility

A complex system model should be able to reproduce experimental results of simple systems. Duan and Sun [31] developed an accurate model (DS model) for CO_2 solubility in water or brine within a wide pressure, temperature, and salinity range. DS model has been comprehensively examined with existing experimental data and is usually treated as a reliable model. We compared this model results for CO_2 solubility with DS model with temperature from 0–250 °C, pressure from 1–1000 bar, and NaCl molality from 0 to saturated condition. Figure 4 shows the comparisons between results from this model and the DS model. From the comparison, this model can reproduce the DS model results with wide TP range at different NaCl concentrations.

To evaluate the influences of $MgCO_3$ dissolution on CO_2 solubility in brine, numerical experiments are conducted with cases of $MgCO_3$ saturated solutions or $MgCO_3$ free solutions at various temperatures and pressures. Figure 5 shows the CO_2 solubility in water with $MgCO_3$ saturated or free conditions. From the comparisons, it can be concluded that dissolution of $MgCO_3$ in water has little influence on CO_2 solubility. This is because of the limited solubility of $MgCO_3$ minerals.

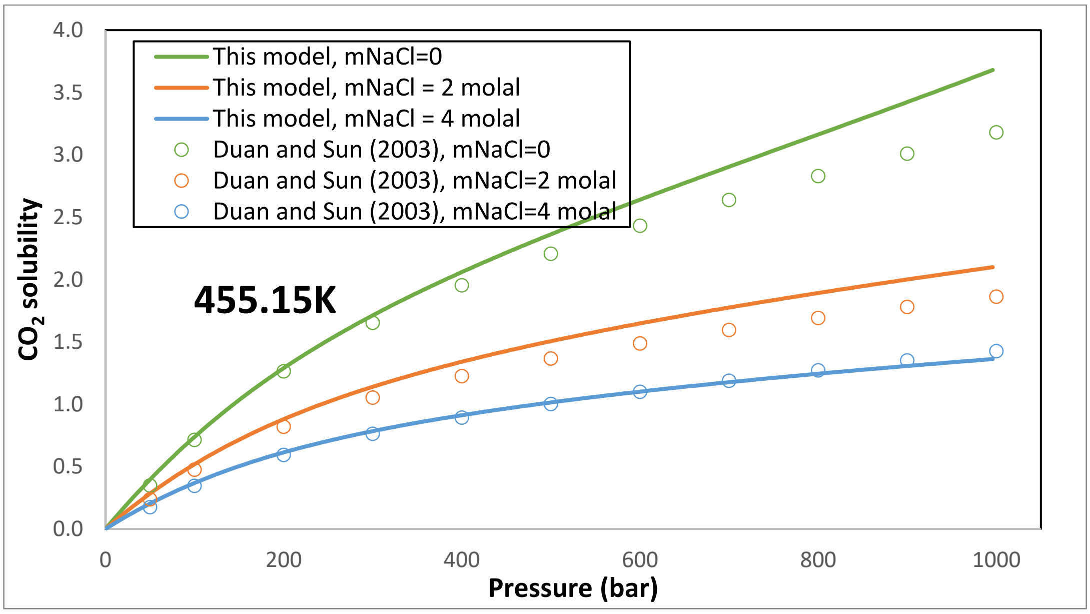

Figure 4. CO_2 solubility varying with pressure at different NaCl concentration calculated by this model (lines) and DS model (dots).

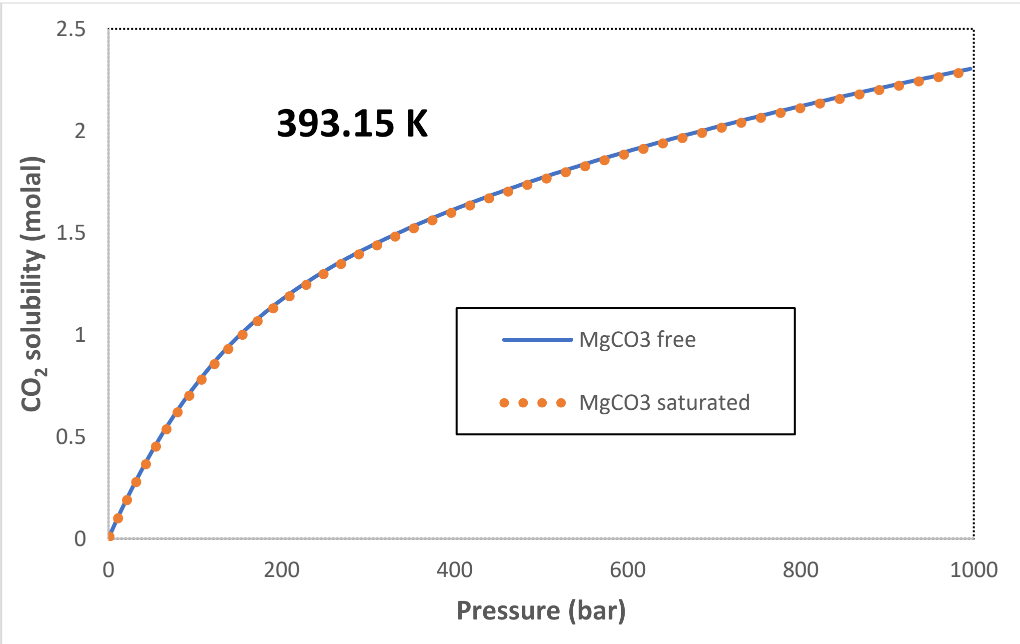

Figure 5. CO_2 solubility varying with pressure at 393.15 K in solutions with $MgCO_3$ saturated (dots) or free (line) conditions.

3.3. Model Predictions

With the new model, the following results can be calculated: (1) the solubility of $MgCO_3$ minerals (i.e., lansfordite, magnesite, and nesquehonite) at various conditions; (2) solutions properties such as pH, various ion concentrations and carbonate concentrations at various conditions of H2O-NaCl-$MgCO_3$-CO_2 systems.

3.3.1. $MgCO_3$ Mineral Solubility

$MgCO_3$ mineral solubilities (i.e., lansfordite, magnesite, and nesquehonite) at various temperatures, pressures, and NaCl molalities are calculated by this model. Figure 6a shows the solubility of magnesite at temperature ranging between 0 and 200 °C, and pressure ranging between 1 and 1000 bar. Magnesite solubility decreases with temperature and increases with pressure. Figure 6b shows the magnesite solubility with CO_2 mole fraction at various temperatures and 100 bar. From the results, the presence of CO_2 in gas phase significantly enhances magnesite solubility in water. Figure 6c shows the magnesite solubility varying with NaCl molalities at 100 bar and various temperatures under conditions of gas free or 100% CO_2. The NaCl molality can enhance the dissolution of magnesite. With same temperature, pressure, and NaCl molality, when the solution is in equilibrium with CO_2, the magnesite solubility increase is significant.

Similar behavior of nesquehonite and lansfordite solubilities are observed from Figure 6d–i at various conditions except temperature effects. Nesquehonite solubility in water decreases with temperature at lower temperature range (about 0–120 °C) and increases with temperature at higher temperature range (about more than 120 °C, Figure 6d). Lansfordite solubility in water increases with temperature with the entire range from 0–200 °C (Figure 6g).

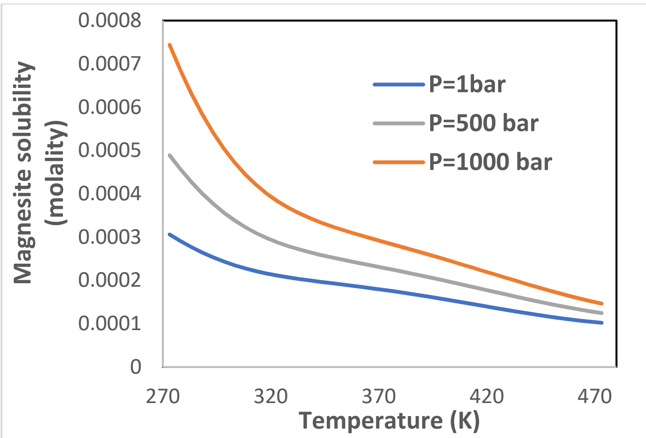

(**a**)

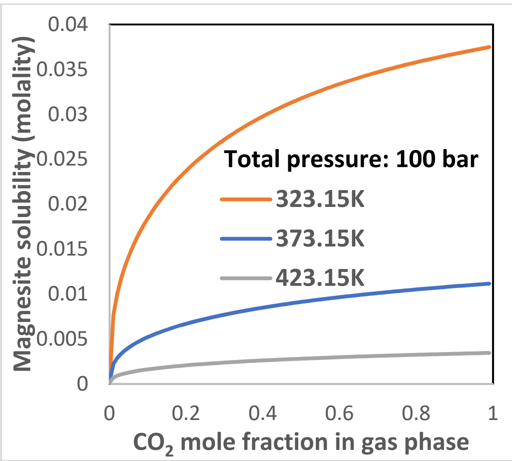

(**b**)

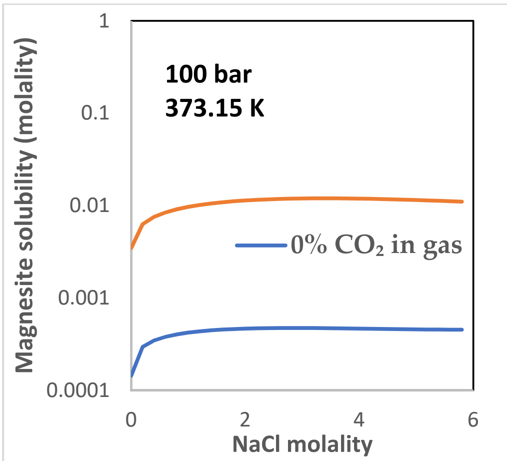

(**c**)

Figure 6. *Cont.*

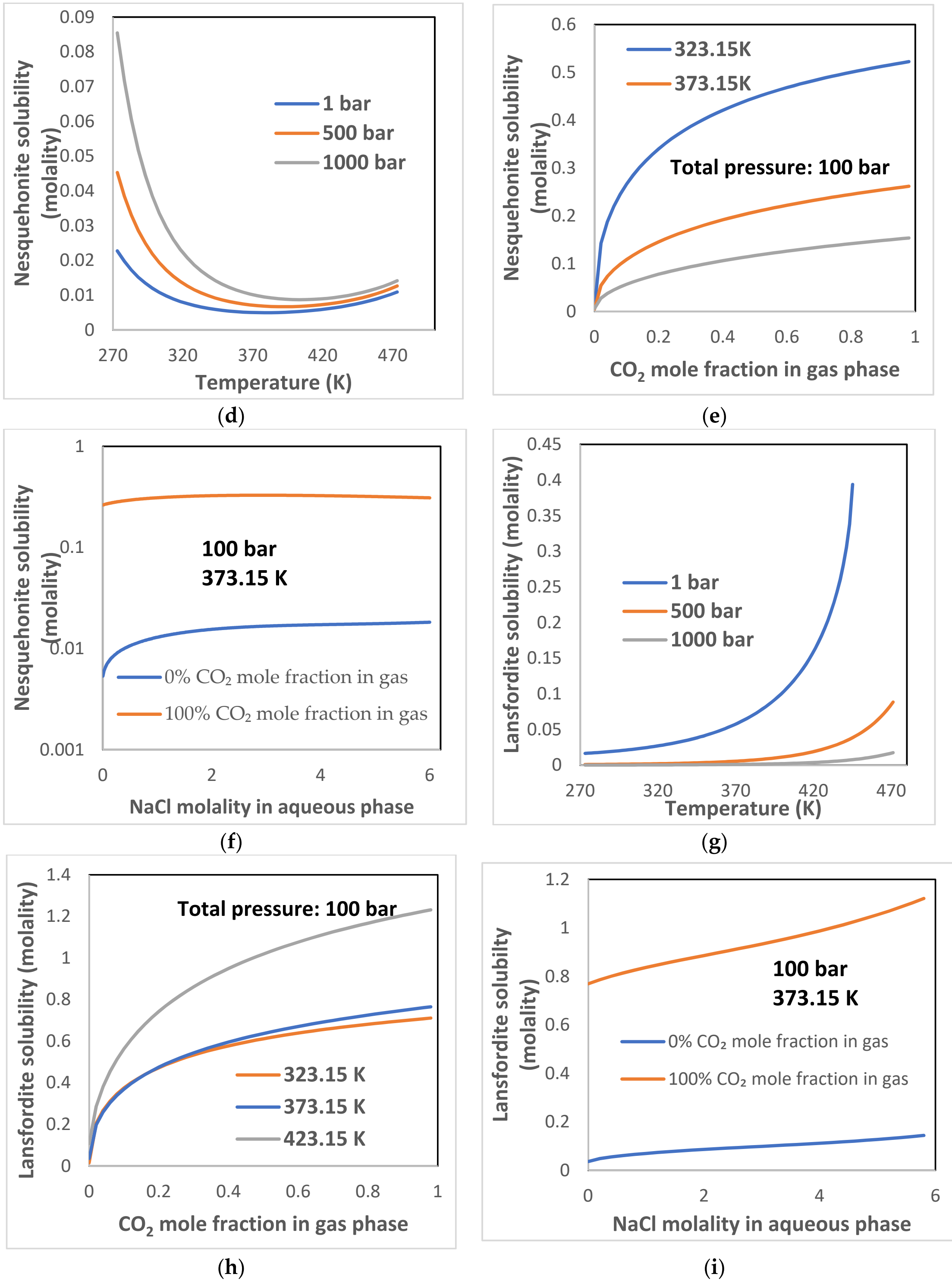

Figure 6. $MgCO_3$ mineral solubility at various temperatures, pressures, NaCl molalitis, and CO2 mole fractions in gas phase. (**a**) Magnesite solubility in water varying with temperature at various pressures; (**b**) magnesite solubility in water varying with CO_2 mole fraction in gas phase at various temperature and 100 bar; (**c**) magnesite solubility in NaCl solutions varying with NaCl molality in cases of 100% CO_2 or 0% CO_2 in gas phase; (**d**) nesquehonite solubility in water varying with temperature at various pressures; (**e**) nesquehonite solubility in water varying with CO_2 mole fraction in gas phase. (**f**) nesquehonite solubility in NaCl solutions varying with NaCl molality; (**g**) lansfordite solubility in water varying with temperature at various pressures; (**h**) lansfordite solubility in water varying with CO_2 mole fraction in gas phase; (**i**) lansfordite solubility in NaCl solutions varying with NaCl molality.

3.3.2. Solution Properties

With the new thermodynamic model of CO_2-H_2O-NaCl-$MgCO_3$ systems, the solution properties (such as pH, various species concentrations, distribution of carbonate species, etc.) can be calculated. Figure 7 shows the pH of solutions (saturated with CO_2) varying with pressure from 1 to 1000 bar at different temperatures under conditions of $MgCO_3$ saturated or free. NaCl molality is 4 molal for all the scenarios. From Figure 7, equilibrium with $MgCO_3$ minerals can significantly increase pH values of the solutions. The $MgCO_3$ minerals can be treated as "buffer minerals" for aqueous solutions.

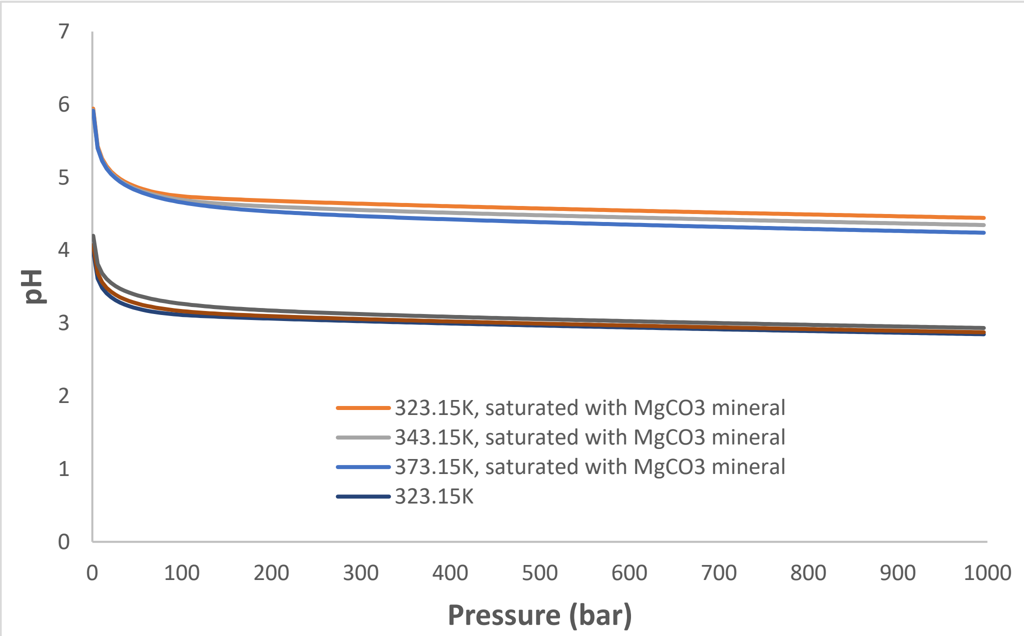

Figure 7. pH of solutions at various temperatures and pressures with or without $MgCO_3$ saturated.

From the previous sections, when CO_2 or carbonate minerals dissolved in water, it can be in the forms of $CO_2^{(aq)}$, HCO_3^-, CO_3^{2-}, and $MgCO_3^{(aq)}$. Figure 8 shows the various carbon species concentrations varying with pressure at 100 °C under conditions of $MgCO_3$ minerals saturated or free. At different conditions, most of the carbon in aqueous solution is in the form of $CO_2^{(aq)}$, and HCO_3^- is secondary. When the solutions are in equilibrium with the $MgCO_3$ minerals, higher concentrations of different forms of carbon can be observed.

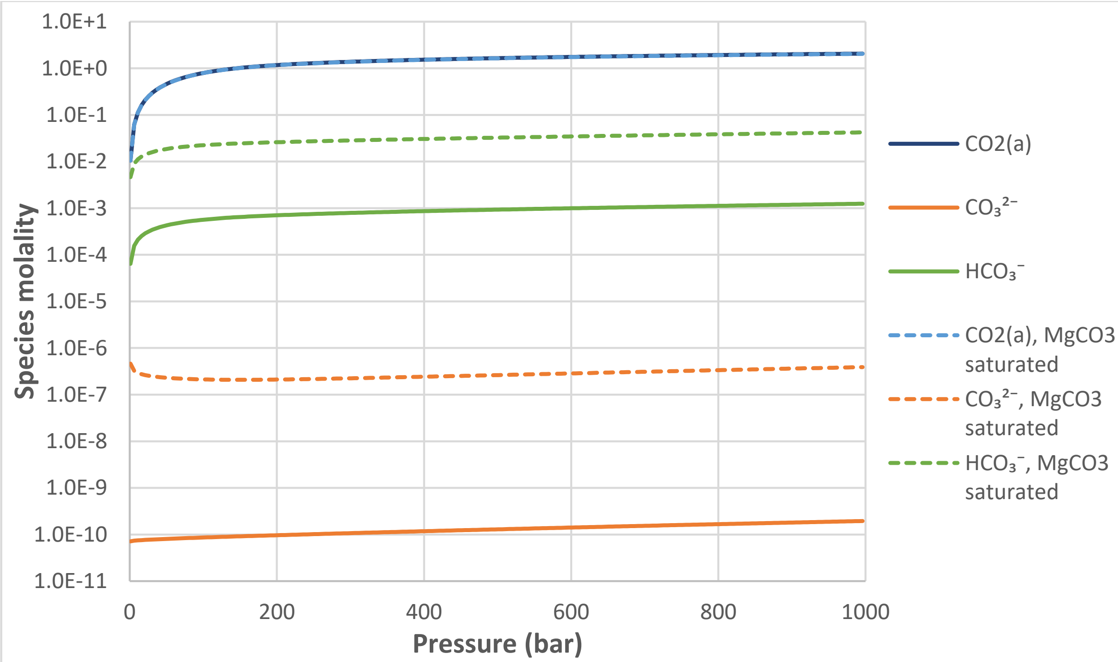

Figure 8. Carbonate concentrations varying with pressure under conditions of $MgCO_3$ saturated or $MgCO_3$ free. The solid lines represent the results with $MgCO_3$ free and dashed lines represent the results with $MgCO_3$ saturated.

4. Conclusions

With regards to the importance of magnesium carbonate minerals to CO_2 geological storage projects, we developed a thermodynamic model of CO_2-H_2O-NaCl-$MgCO_3$ systems from 0–200 °C, 1–1000 bar, and halite up to high concentration. The model can calculate the phase equilibria and speciation including gas phase mole fractions, molality of aqueous species (such as $CO_3{}^{2-}$, $HCO_3{}^-$, Mg^{2+}, $Mg(OH)^+$, H^+, OH^-, $CO_2{}^{(aq)}$, and $MgCO_3{}^{(aq)}$), pH, and dissolution and precipitation of $MgCO_3$ minerals.

To validate the model, we compared the model results with the current existing data in terms of CO_2 solubility in aqueous solutions, and $MgCO_3$ mineral solubilities. From the comparison, CO_2 solubility in NaCl solutions can be reproduced in a wide temperature, pressure, and salinity range with similar accuracy as the previous work [31,46]. The experimental solubility of nesquehonite, magnesite, and lansfordite in aqueous solutions with various temperature and CO_2 partial pressure can be reproduced by this model. The *AAD*% between model results and experimental data are calculated. From the results, most of the experimental data can be reproduced with *AAD*% less than 10%.

The model is used for the prediction of phase equilibria of CO_2-H_2O-NaCl-$MgCO_3$ systems with temperature from 0–200 °C, pressure from 1–1000 bar, and halite concentration up to 6 molal. From the results, the followings can be concluded.

(1) Temperature usually decreases the mineral solubilities, and pressure usually increases the solubility. However, for nesquehonite, the solubility decreases with temperature when the temperature is less than about 100 °C and increases when the temperature is higher than 100 °C. For lansfordite, the solubility increases with temperature from 0–200 °C.
(2) The presence of CO_2 in aqueous solution or gases phase will significantly enhance the dissolution of $MgCO_3$ minerals.
(3) For CO_2 saturated solutions, the dissolution of $MgCO_3$ minerals will increase the pH of the solutions at different temperature and pressure conditions. $MgCO_3$ minerals can be treated as "buffer minerals".

(4) The influences of $MgCO_3$ minerals on CO_2 solubility are insignificant. However, the concentrations of carbon-bearing ions in the solutions are significantly increased by the dissolution of $MgCO_3$ minerals.

Author Contributions: Conceptualization, methodology, validation, investigation, resources, data curation, and writing—original draft preparation, J.L.; writing—review and editing, X.L. and J.L.

Funding: This research was funded by National Natural Science Foundation of China (Grant No. 41502246) and National Key R&D Program of China (Grant No. 2016YFE0102500).

Conflicts of Interest: The authors declare no conflict of interest.

References

1. Zhao, H.; Liao, X.; Chen, Y.; Zhao, X. Sensitivity analysis of CO_2 sequestration in saline aquifers. *Pet. Sci.* **2010**, *7*, 372–378. [CrossRef]
2. Li, J.; Ahmed, R.; Li, X. Thermodynamic modeling of CO_2-N_2-O_2-Brine-Carbonates in conditions from surface to high temperature and pressure. *Energies* **2018**, *11*, 2627. [CrossRef]
3. Bénézeth, P.S.; Saldi, G.D.; Dandurand, J.-L.; Schott, J. Experimental determination of the solubility product of magnesite at 50 to 200 °C. *Chem. Geol.* **2011**, *286*, 21–31. [CrossRef]
4. Li, J.; Li, X. Analysis of u-tube sampling data based on modeling of CO_2 injection into CH4 saturated aquifers. *Greenh. Gases: Sci. Technol.* **2015**, *5*, 152–168. [CrossRef]
5. Wagner, R. Ueber die löslichkeit einiger erd-und metallcarbonate in kohlensäurehaltigem wasser. *J. Anal. Chem.* **1867**, *6*, 233–238. [CrossRef]
6. Cameron, F.K.; Briggs, L.J. Equilibrium between carbonates and bicarbonates in aqueous solution. *J. Phys. Chem.* **1901**, *5*, 537–555. [CrossRef]
7. Wells, R.C. The solubility of magnesium carbonate in natural waters.2. *J. Am. Chem. Soc.* **1915**, *37*, 1704–1707. [CrossRef]
8. Bär, O. Beitrag zum thema dolomitentstehung. *Zentr. Mineral. Geol. Palaontol. Abt. A* **1932**, *1932*, 46–62.
9. Halla, F.; Chilingar, G.V.; Bissell, H.J. Thermodynamic studies on dolomite formation and their geologic implications: An interim report. *Sedimentology* **1962**, *1*, 296–303. [CrossRef]
10. Berg, L.G.; Borisova, L.A. Solubility isotherms of the ternary systems Mg^{2+}, Ca^{2+}//$CO_3{}^{2-}$, H_2O, Na^+, Ca^{2+}//$CO_3{}^{2-}$, H_2O and Na^+, Mg^{2+}//$CO_3{}^{2-}$, H_2O at 25 °C and P_{CO2} = 1 atmosphere. *Russ. J. Inorg. Chem.* **1960**, *5*, 618–620.
11. Christ, C.L.; Hostetler, P.B. Studies in the system MgO-SiO_2-CO_2-H_2O (ii); the activity-product constant of magnesite. *Am. J. Sci.* **1970**, *268*, 439–453. [CrossRef]
12. Cameron, F.K.; Seidell, A. The solubility of magnesium carbonate in aqueous solutions of certain electrolytes. *J. Phys. Chem.* **2002**, *7*, 578–590. [CrossRef]
13. Engel, M. Sur la solubilité des sels en présence des acides, des bases et de sels. *Ann. Chim. Phys.* **1889**, *17*, 349–369.
14. Königsberger, E.; Königsberger, L.-C.; Gamsjäger, H. Low-temperature thermodynamic model for the system $Na_2CO_3-MgCO_3-CaCO_3-H_2O$. *Geochim. Cosmochim. Acta* **1999**, *63*, 3105–3119. [CrossRef]
15. Kline, W.D. The solubility of magnesium carbonate (nesquehonite) in water at 25 °C and pressures of carbon dioxide up to one atmosphere1. *J. Am. Chem. Soc.* **1929**, *51*, 2093–2097. [CrossRef]
16. Mitchell, A.E. Ccxii.—studies on the dolomite system.—Part ii. *J. Chem. Soc. Trans.* **1923**, *123*, 1887–1904. [CrossRef]
17. Haehnel, O. Über die löslichkeit des magnesiumcarbonats in kohlensäurehaltigem wasser unter höheren kohlendioxyddrucken und über die eigenschaften solcher magnesiumbicarbonatlösungen. *J. für Prakt. Chem.* **1924**, *108*, 61–74. [CrossRef]
18. Yanat'eva, O.K. Solubility of the system Ca, Mg-CO_3, SO_4-H_2O at 25 °C and P_{CO2} of 0.0012 atm. *Zh. Neorgan. Khim.* **1957**, *2*, 2183–2187.
19. Takahashi, G. Investigation on the synthesis of potassium carbonate by Mr. Engel. *Bull. Imp. Hyg. Lab. (Tokyo)* **1927**, *29*, 165–262.
20. Ponizovskii, A.M.; Vladimirova, N.M.; Gordon-Yanovskii, F.A. The solubility relation in the system Na, Mg-Cl, HCO_3-H_2O at 0°C with carbon dioxide at 4 and 10 kg/cm^2. *Russ. J. Inorg. Chem.* **1960**, *5*, 1250–1252.

21. Yanat'eva, O.K.; Rassonskaya, I.S. Metastable equilibria and solid phases in the $CaCO_3$-$MgCO_3$-H_2O system. *Russ. J. Inorg. Chem.* **1961**, *6*, 730–733.
22. Harvie, C.E.; Weare, J.H. The prediction of mineral solubilities in natural waters: The Na-K-Mg-Ca-Cl-SO_4-H_2O system from zero to high concentration at 25 °C. *Geochim. Cosmochim. Acta* **1980**, *44*, 981–997. [CrossRef]
23. Harvie, C.E.; Møller, N.; Weare, J.H. The prediction of mineral solubilities in natural waters: The Na-K-Mg-Ca-H-Cl-SO_4-OH-HCO_3-CO_3-CO_2-H_2O system to high ionic strengths at 25 °C. *Geochim. Cosmochim. Acta* **1984**, *48*, 723–751. [CrossRef]
24. Pitzer, K.S. Thermodynamics of electrolytes. I. Theoretical basis and general equations. *J. Phys. Chem.* **1973**, *77*, 268–277. [CrossRef]
25. Pitzer, K.S.; Mayorga, G. Thermodynamics of electrolytes. II. Activity and osmotic coefficients for strong electrolytes with one or both ions univalent. *J. Phys. Chem.* **1973**, *77*, 2300–2308. [CrossRef]
26. Pitzer, K.S.; Kim, J.J. Thermodynamics of electrolytes. IV. Activity and osmotic coefficients for mixed electrolytes. *J. Am. Chem. Soc.* **1974**, *96*, 5701–5707. [CrossRef]
27. Pitzer, K.S. Thermodynamic properties of aqueous sodium chloride solutions. *J. Phys. Chem. Ref. Data* **1984**, *13*, 1–102. [CrossRef]
28. Møller, N. The prediction of mineral solubilities in natural waters: A chemical equilibrium model for the Na-Ca-Cl-SO_4-H_2O system, to high temperature and concentration. *Geochim. Cosmochim. Acta* **1988**, *52*, 821–837. [CrossRef]
29. Greenberg, J.P.; Møller, N. The prediction of mineral solubilities in natural waters: A chemical equilibrium model for the Na-K-Ca-Cl-SO_4-H_2O system to high concentration from 0 to 250 °C. *Geochim. Cosmochim. Acta* **1989**, *53*, 2503–2518. [CrossRef]
30. Christov, C.; Moller, N. Chemical equilibrium model of solution behavior and solubility in the H-Na-K-OH-Cl-HSO_4-SO_4-H_2O system to high concentration and temperature.11 associate editor: Wesolowski. D. *J. Geochim. Cosmochim. Acta* **2004**, *68*, 1309–1331. [CrossRef]
31. Duan, Z.; Sun, R. An improved model calculating CO_2 solubility in pure water and aqueous NaCl solutions from 273 to 533 K and from 0 to 2000 bar. *Chem. Geol.* **2003**, *193*, 257–271. [CrossRef]
32. Duan, Z.; Li, D. Coupled phase and aqueous species equilibrium of the H2O–CO_2–NaCl–$CaCO_3$ system from 0 to 250 °C, 1 to 1000 bar with NaCl concentrations up to saturation of halite. *Geochim. Cosmochim. Acta* **2008**, *72*, 5128–5145. [CrossRef]
33. Li, D.; Duan, Z. The speciation equilibrium coupling with phase equilibrium in the H2O–CO_2–NaCl system from 0 to 250 °C, from 0 to 1000 bar, and from 0 to 5 molality of NaCl. *Chem. Geol.* **2007**, *244*, 730–751. [CrossRef]
34. Li, J.; Duan, Z. A thermodynamic model for the prediction of phase equilibria and speciation in the H_2O–CO_2–NaCl–$CaCO_3$–$CaSO_4$ system from 0 to 250 °C, 1 to 1000 bar with NaCl concentrations up to halite saturation. *Geochim. Cosmochim. Acta* **2011**, *75*, 4351–4376. [CrossRef]
35. Parkhurst, D.L.; Appelo, C.A.J. User's guide to PHREEQC (Version 2)—A computer program for speciation, batch-reaction, one-dimensional transport, and inverse geochemical calculations. *Water-Resour. Investig. Rep.* **1999**, *99*, 312.
36. Xu, T.; Spycher, N.; Sonnethal, E.; Zhang, G.; Zheng, L.; Pruess, K. TOUGHREACT Version 2.0: A simulator for subsurface reactive transport under non-isothermal multiphase flow conditions. *Comput. Geosci.* **2011**, *37*, 763–774. [CrossRef]
37. Su, D.; Mayer, K.U.; MacQuarrie, K.T. Parallelization of MIN3P-THCm: A high performance computational framework for subsurface flow and reactive transport simulation. *Environ. Model. Softw.* **2017**, *95*, 271–289. [CrossRef]
38. Wolery, T.J. EQ3/6 A Software Package for Geochemical Modeling (Version 05). Report Number: LLNL-CODE-638958. Available online: https://www.osti.gov//servlets/purl/1231666 (accessed on 28 November 2019).
39. Zhu, C.; Burden, D.S. Mineralogical compositions of aquifer matrix as necessary initial conditions in reactive contaminant transport models. *J. Contam. Hydrol.* **2001**, *51*, 145–161. [CrossRef]
40. Dobson, P.; Salah, S.; Spycher, N.; Sonnenthal, E.L. Simulation of Water-Rock interaction in the Yellowstone Geothermal system using TOUGHREACT. *Geochermics* **2004**, *33*, 493–502. [CrossRef]

41. Zhang, W.; Shi, W.; Li, J.; Deng, G.; Chang, Y.; Li, Z. Application of geochemical code EQ3/6 to leaching technique of hard rock uranium deposit. *J. East. China Geol. Inst.* **1997**, *20*, 362–367.
42. *Computer Modeling Group (CMG), User Technical Manual*; Computer Modelling Group Ltd.: Calgary, Canada, 2016.
43. Wei, L. Sequential Coupling of Geochemical Reactions With Reservoir Simulations for Waterflood and EOR Studies. *SPE J.* **2012**, *17*, 469–484. [CrossRef]
44. Adegbite, J.O.; Al-Shalabi, E.W.; Ghosh, B. Modeling the Effect of Engineered Water Injection on Oil Recovery from Carbonate Cores. In Proceedings of the SPE International Conference on Oilfield Chemistry, Montgomery, TX, USA, 3–5 April 2017. [CrossRef]
45. Li, X.; Wei, L.; Zhang, H. Improving Reactive Transport Modeling Predictivity for ASP Flooding Simulations. In Proceedings of the SPE EOR Conference at Oil and Gas West Asia, Muscat, Oman, 21–23 March 2016; pp. 1–20. [CrossRef]
46. Li, J.; Wei, L.; Li, X. An improved cubic model for the mutual solubilities of CO_2–CH_4–H_2S–brine systems to high temperature, pressure and salinity. *Appl. Geochem.* **2015**, *54*, 1–12. [CrossRef]
47. Appelo, C.A.J.; Parkhurst, D.L.; Post, V.E.A. Equations for calculating hydrogeochemical reactions of minerals and gases such as CO_2 at high pressures and temperatures. *Geochim. Cosmochim. Acta* **2014**, *125*, 49–67. [CrossRef]
48. Helgeson, H.C.; Kirkham, D.H.; Flowers, G.C. Theoretical prediction of the thermodynamic behavior of aqueous electrolytes at high pressures and temperatures: Calculation of activity coefficients, osmotic coefficients, and apparent molal and standard and relative partial modal properties to 600 °C and 5 Kb. *Am. J. Sci.* **1981**, *281*, 1249–1516. [CrossRef]
49. Duan, Z.; Sun, R.; Zhu, C.; Chou, I.M. An improved model for the calculation of CO_2 solubility in aqueous solutions containing Na^+, K^+, Ca^{2+}, Mg^{2+}, Cl^-, and $SO_4{}^{2-}$. *Mar. Chem.* **2006**, *98*, 131–139. [CrossRef]
50. Peng, D.-Y.; Robinson, D.B. A new two-constant equation of state. *Ind. Eng. Chem. Fundam.* **1976**, *15*, 59–64. [CrossRef]
51. Michelsen, M.L.; Mollerup, J.M. *Thermodynamic models: Fundamentals & Computational Aspects*, 2nd ed.; TIE-LINE Publications: Herning, Denmark, 2007.
52. Visscher, A.D.; Vanderdeelen, J.; Königsberger, E.; Churagulov, B.R.; Ichikuni, M.; Tsurumi, M. Iupac-nist solubility data series. 95. Alkaline earth carbonates in aqueous systems. Part 1. Introduction, be and mg. *J. Phys. Chem. Ref. Data.* **2012**, *41*, 013105. [CrossRef]